

# Pattern recognition for partial discharge in GIS based on pulse coupled neural networks and wavelet packet decomposition

**Abstract.** Based on the characteristics of partial discharge (PD) defects in gas insulated switchgear (GIS), four typical single defects were designed for the present paper. PD three-dimensional (3D) patterns were constructed based on the ultra high frequency detection systems. The pulse-coupled neural networks (PCNN) and wavelet packet decomposition (WPD) method were used in PD feature extraction. The recognition results show that the proposed method used in PD feature extraction can effectively improve the accuracy of pattern recognition rate.

**Streszczenie.** Przeanalizowano defekty wyłącznika gazowego z wyładowaniem niezupełnym. Defekty te przedstawiane są jako obrazy 3D. Do ekstrakcji cech tych obrazów wykorzystuje się transformatę falkową i impulsowo sprzężone sieci neuronowe. (Rozpoznawanie cech wyładowania niezupełnego w wyłącznikach gazowych z wykorzystaniem impulsowo sprzężonych sieci neuronowych i transformaty falkowej)

**Keywords:** gas insulated switchgear, partial discharge, pulse coupled neural networks, wavelet packet decomposition.

**Słowa kluczowe:** in the case of foreign Authors in this line the Editor inserts Polish translation of keywords.

## Introduction

Gas insulated switchgear (GIS) has been widely used all over the world, the high reliability, low maintenance and compact size made it an attractive choice in many cases. Though GIS has high reliability, the return of practical experience indicated that most of the failures are related to insulation problems. Partial discharge (PD) is one of the main reasons for causing internal insulation deterioration of GIS [1-4]. Online monitoring of PD can promptly and accurately determine the status of the internal insulation to prevent GIS accidents and ensure power system security and stability.

Conventional PD measurement using the pulse-current method is vulnerable to low-frequency electromagnetic field interference; therefore, the ultra high frequency (UHF) method of detecting PD signals has been extensively used.

Johnson studied the feasibility of using pulse-coupled neural networks (PCNN) for target image feature extraction at the earliest stage in 1993; later Raul, Godin, Karvonen and others, also performed similar research and explorations [5-8]. Waldemark et al. [9] conducted the PCNN segmentation-based hybrid neural network automatic classification of military targets. Previous studies [10]-[11] utilized PCNN geometric transformation (e.g., translation, rotation, shrink, etc.) with the same characteristics to achieve the goal of target image classification.

Wavelet packet decomposition (WPD) [12-15] has abilities in decomposition of low-frequency part, and the decomposition of high frequency part in multi-resolution analysis. The main advantage of wavelet packet decomposition is wavelet packet can portray a more detailed characterization of high-frequency part, stronger analysis of the signal.

In the current paper, we designed four typical physical models of defects in GIS, after which the PD 3D patterns are constructed. The PCNN and WPD method is used in the GIS PD pattern recognition. This method can extract the information entropy from the PD gray matrix and then calculate the WPC energy of entropy as the categorizing feature. The recognition results show that this algorithm can extract entropy-sequence features of PD samples and improve the accuracy of pattern recognition.

## PCNN model

PCNN is a feedback network formed by the connection of many neurons according to the elicitation of biological visual cortex patterns. The basic model of the PCNN

neuron comprises three parts, namely, receptive field, modulation field, and pulse generator.

The discrete mathematical equations of each neural network are described as follows:

$$(1) F_{ij}(n) = e^{-\alpha_F} F_{ij}(n-1) + V_F \sum_{kl} M_{ijkl} Y_{kl}(n-1) + S_{ij}$$

$$(2) L_{ij}(n) = e^{-\alpha_L} L_{ij}(n-1) + V_L \sum_{kl} W_{ijkl} Y_{kl}(n-1)$$

$$(3) U_{ij}(n) = F_{ij}(n)(1 + \beta L_{ij}(n))$$

$$(4) Y_{ij}(n) = \begin{cases} 1, & U_{ij}(n) > E_{ij}(n-1) \\ 0, & \text{otherwise} \end{cases}$$

$$(5) E_{ij}(n) = e^{-\alpha_E} E_{ij}(n-1) + V_E Y_{ij}(n)$$

where equations (1), (2), and (3) are the mathematical models of the receptive feeding input, receptive linking input and modulating coupler, respectively; and equations (4) and (5) are the expressions of variable threshold function and the step function of the pulse generator, respectively. In equations (1)-(5),  $i$  is the  $i$ -th linking input neuron,  $j$  is the  $j$ -th neuron,  $S_{ij}$  is the input signal,  $F_{ij}$  is the feeding input,  $L_{ij}$  is the linking input,  $U_{ij}$  is the internal activity, and  $E_{ij}$  is the dynamic threshold. Meanwhile, matrices  $M_{ijkl}$ ,  $W_{ijkl}$ , and  $V_E$  are the linking weight/magnification coefficients of the feeding back field and the linking field, as well as the threshold magnification coefficient, respectively. In addition,  $\alpha_F$ ,  $\alpha_L$ , and  $\alpha_E$  are the decay constants associated with  $F$ ,  $L$  and  $E$ , respectively; and  $\beta$ ,  $n$ , and  $Y_{ij}$  are the connection coefficient, the iteration number and the pulse output, respectively.

Entropy is a form of image demographic characteristics, which reflects the amount of information included in an image. Based on the Shannon entropy definition, the binary image entropy can be calculated as follows:

$$(6) En[n] = -P_1 \log_2(P_1) - P_0 \log_2(P_0)$$

where  $En[n]$  indicates the information entropy of the binary image, and  $P_1$  and  $P_0$  indicate the probability of one and zero, respectively.

Due to the difference between the corresponding sequence entropy and time distribution, the distribution curves of the entropy sequences are also different.

## Wavelet packet decomposition

As the scaling function  $\Phi(t)$  and wavelet function  $\Psi(t)$  has two scale relations:

$$(7) \begin{cases} \phi(t) = \sum_k h_k \phi(2t-k) \\ \Psi(t) = \sum_k g_k \phi(2t-k) \end{cases}$$

The function series  $\{\phi_l(t)\}_{l \in \mathbb{Z}^+}$  defined by equations

(7) can be called orthogonal wavelet packet determined by  $\Phi_0(t) = \Phi(t)$ , expressed as:

$$(8) \begin{cases} \phi_{2m}(t) = \sum_k h_k \phi_m(2t-k) \\ \phi_{2m+1}(t) = \sum_k g_k \phi_m(2t-k) \end{cases}$$

The wavelet packet coefficients (WPC) of each node  $(j, m)$  can be calculated by time series  $x(t)$  as:

$$(9) C_{j,m}(k) = \langle x(t), \phi(2t-k) \rangle$$

WPC  $C_{j,m}(k)$  contains all information of a reconstruction signal, the square value represents the energy of certain branch signals in the wavelet packet tree.

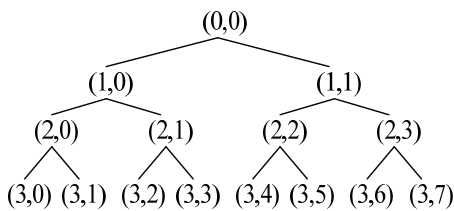


Fig. 1. Tree structure of WPD at level 3.

At each level  $j$ , the detail coefficients are also filtered by  $h_k$  and  $g_k$ . In the framework of the WPD, there is no more need to maintain the difference between approximation and detail coefficients because both of them are now treated in the same way. For a  $j=3$  WPD, the full filtering tree of Fig.1 is obtained.

#### PCNN and WPD feature-extraction process

In the PD  $\varphi\text{-}q\text{-}n_p$  3D image coordinate axis (where  $\varphi$  is the power frequency phase position,  $q$  is the discharge amplitude, and  $n_p$  is the PD count),  $n_p$  can be regarded as the gray value of the 2D image with coordinate axis  $\varphi\text{-}q$ . Based on the proposed PCNN entropy-sequence algorithm and WPD, the steps in combining the characteristics of the PD image are as follows:

(1) The  $n$ -axis of the four types of PD 3D images is normalized to  $[0, 1]$ , according to Steps (2)–(5), followed by the PCNN entropy-sequence algorithm and WPD.

(2) By assuming that the resolution of the normalized PD 3D image is  $p_1 \times p_2$ , the image is converted to  $p = p_1 \times p_2$  dimensional image vector  $A_i$ . Meanwhile,  $M$  samples constitute the sample set  $\{A_1, A_2, \dots, A_M\}$ .

(3) The initial value of the PCNN parameters is set, putting each pixel in the extinguished state. Data from the sample set  $\{A_1, A_2, \dots, A_M\}$  are read, scanning operations for the pixel matrix are carried out, and PCNN generates the timing pulse sequence. After each end of scan, the information entropy of  $Y_{ij}(n)$  is obtained using equations (4). After several scanning operations, the corresponding output is the entropy sequence  $E_n[n]$ .

(4) The obtained entropy sequence  $E_n[n]$  is decomposed by three layer wavelet packet, extracted eight signal characteristics from low to high frequency components in the third layer. The WPC are reconstructed,

extracting the entropy signals of each frequency range to calculate the energy of reconstructed signals as PD feature.

(5) Classification and identification are conducted using the back propagation (BP) neural network; the PD characteristic vectors are BP neural network inputs, the training method used is the orthogonal least square method.

#### Defect models in GIS

Physical models of four typical single defects were designed based on the characteristics and features of PD in GIS. Fig. 2 shows the physical models of these defects.

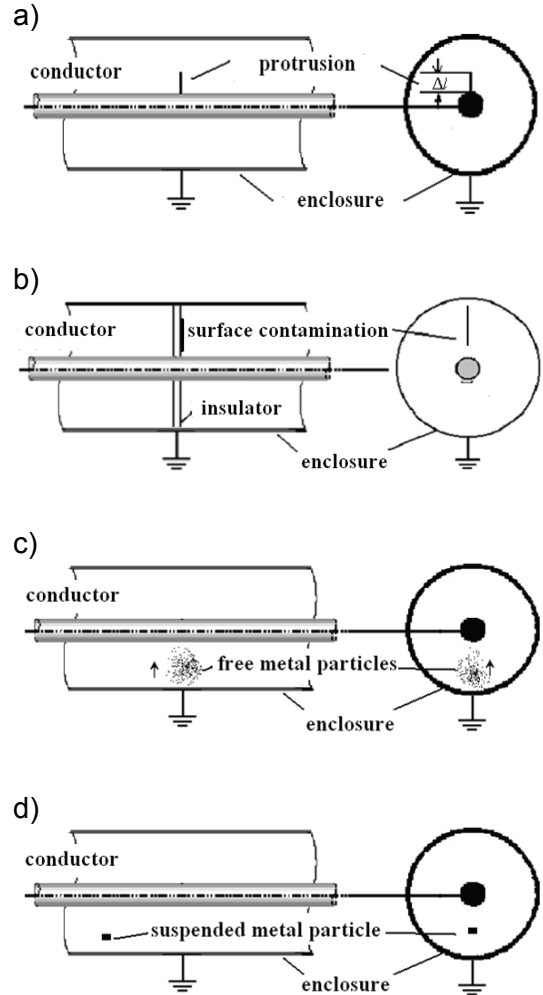


Fig.2. Physical models of the defects in GIS: a) protrusion fixed to the conductor discharge model, b) surface contamination on the insulator discharge model, c) free metal particles discharge model, d) suspended metal particle discharge model

Fig. 2a shows the protrusion fixed to the conductor discharge model. A shiny copper wire (diameter of 1.0mm) is fixed to the conductor to simulate this type of defect. The length of the copper wire can be adjusted according to the applied voltage in the testing. In the experiment, the distance between the wire tip and enclosure is 10mm. Fig. 2b shows the surface contamination on the insulator discharge model, a thin copper wire (length of 50mm, diameter of 0.1mm), which adheres to the cone type insulating spacer, is used to simulate this defect. The distance between copper wire and high voltage conductor is 10mm. Fig. 2c shows the free metal particles discharge model. The PD of the free metal particles depended on the

nature of the material, the size of the metal particles, and the applied voltage. In the experiments, rectangular aluminum metal particles ( $2\text{mm} \times 2\text{mm}$ , thickness of  $0.1\text{mm}$ ) is used and placed in the enclosure. Fig. 2d shows the suspended metal particle discharge model, a stainless steel hex bolt (length of  $50\text{mm}$ , diameter of  $8.8\text{mm}$ ) which hangs to the conductor, is used to simulate this defect. The distance between the hex bolt and conductor is  $40\text{mm}$ .

### PD 3D patterns of the four types of defects

The PD experiments were carried on  $110\text{kV}$  three-phase GIS test platform, applied voltage acted on single phase when the experiments started, the  $\text{SF}_6$  gas pressure in GIS was  $0.6\text{MPa}$  (show as Fig.3). Fig. 4 shows the schematic of the experimental circuit for PD detection in GIS, T1 is a  $0-380\text{ V}$  induction voltage regulator, T2 is a  $1000\text{ kV}/5\text{A}$  testing transformer without corona, C1 and C2 constitutes the capacitive voltage divider, R is a  $10\text{ k}\Omega$  protective resistance,  $R_d$  is a  $50\Omega$  measurement resistance,  $C_x$  is the GIS test model. Experiments were conducted using a high-performance medium filled antenna. The antenna had a frequency range of  $400-1500\text{ MHz}$ , and a UHF voltage standing-wave ratio of less than two. The applied  $50\text{ Hz}$  ac voltage was manually increased from  $0$  to  $1000\text{ kV}$  peak. PD was generated by simultaneously applying high ac voltage above the discharge inception level of GIS. The PD signals were measured with a DTS 7104 oscilloscope, which had a  $1\text{ GHz}$  bandwidth and a maximum sampling rate of  $20\text{ Gs}$ . Using ultra wide-band detection techniques coupled with rapid oscilloscope acquisition, the true PD pulse shape was recorded, and the shape of the individual PD pulse was observed.

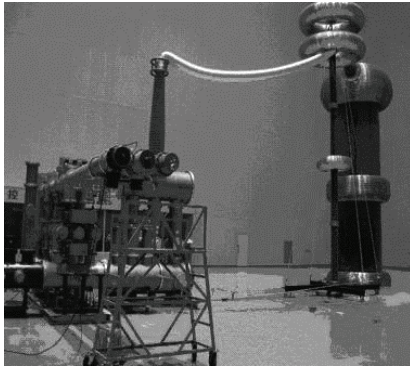


Fig.3.  $110\text{kV}$  GIS PD test platform

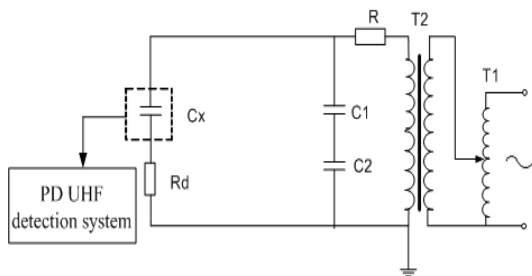
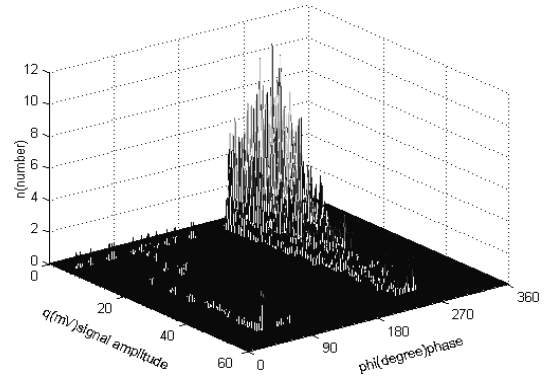


Fig.4. Experimental circuit schematic for PD detection in  $110\text{kV}$  GIS

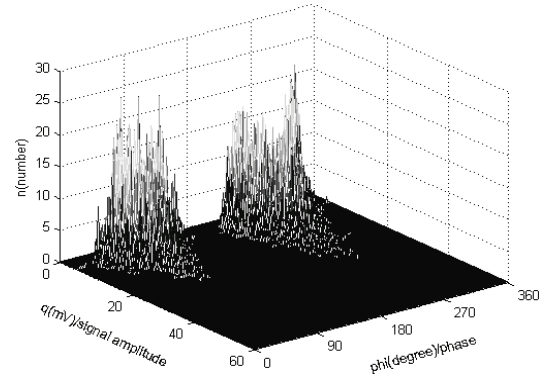
The medium filled antenna was used to collect PD signals and simultaneously obtain cycle frequency signals from the capacitive divider to provide phase information. The sampling rate was  $250\text{ Ms}$ , which collected  $50$  frequency cycles to constitute PD 3D pattern samples; the

resolution of the patterns was  $128 \times 256$ . The patterns of the four typical defects are shown in Fig. 5.

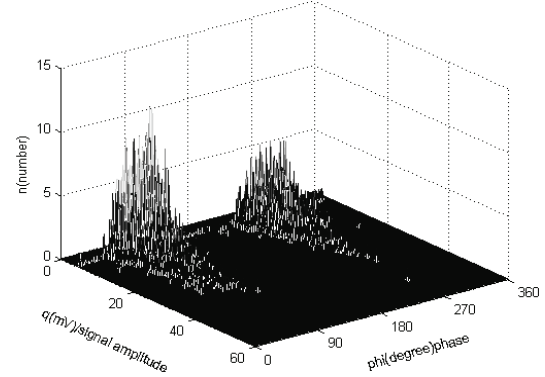
a)



b)



c)



d)

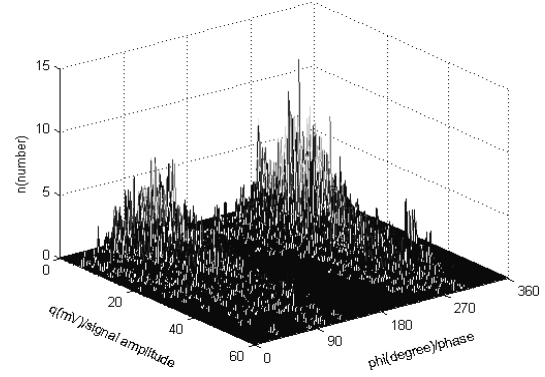


Fig.5. Typical PD  $\varphi$ - $q$ - $n_p$  distributions: a) protrusion fixed to the conductor discharge, b) surface contamination on the insulator discharge, c) free metal particles discharge, d) suspended metal particle discharge

## Test and recognition results

Test samples were obtained from the four types of discharge defect models, which were acquired using different test voltages. There were 150 effective PD samples from each type of defect, of which 50 samples were used as the training samples, and the remaining 100 samples were used for testing.

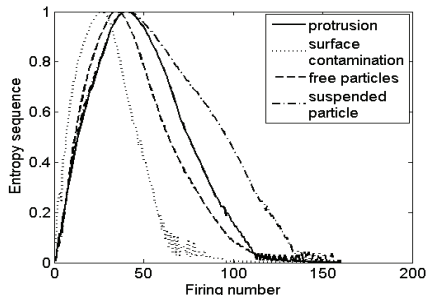


Fig.6. PCNN output entropy sequence

Table 1. WPC energy of four typical defects in GIS

Node	Protrusion	Surface contamination	Free particles	Suspended particle
(3,0)	6.5537	7.5133	5.9772	5.2346
(3,1)	0.10074	0.11974	0.11278	0.14999
(3,2)	0.029469	0.023039	0.017183	0.077042
(3,3)	0.044484	0.034567	0.039632	0.087374
(3,4)	0.036211	0.045606	0.014134	0.10522
(3,5)	0.025559	0.025726	0.0065635	0.049542
(3,6)	0.013815	0.014616	0.0068363	0.057138
(3,7)	0.018764	0.040869	0.0089012	0.067972

Fig. 6 shows the outputs entropy sequences of PD 3D grayscale images by PCNN method at  $\beta=0.8$ , through the calculation of frequency components energy as PD identification features, the typical calculation results list in Table 1. Among them, WPC energy of node (3,0), (3,4), (3,5), (3,6), (3,7) are great difference between each other, helpful for the following classification and identification.

The recognition rates of the proposed method for various defects are over 87% (Table 2), indicating that this method has high recognition rate and good effect.

Table 2. Recognition results of five typical single defects in GIS

Defect types	Number of training samples	Number of test samples	Test voltage (kV)	Recognition rate (%)
Protrusion	50	100	30	91.7
Surface contamination	50	100	26	89.6
Free particles	50	100	22	87.6
Suspended particle	50	100	18	94.4

## Conclusions

The physical models of four typical defects in GIS have been designed. Many PD samples are acquired using a medium filled antenna and high-speed sampling system. In addition, PD 3D patterns are constructed in the experiments. The PCNN and WPD method are applied to pattern recognition of PD 3D images because the entropy-sequence curve of the PCNN output binary images varies with the image gray pixel value distribution, and WPC energy have great difference between each other. The recognition results from the extracted WPC energy for entropy-sequence as characteristics using PCNN and WPD method of the PD 3D images prove that this algorithm is effective.

## Acknowledgment

The authors would like to thank the National Basic Research Program of China (Project No. 2009CB724506) and the Fundamental Research Funds for the Central Universities (Project No. CDJXS11152234) for the financial support.

## REFERENCES

- [1] Chang C., Chang C.S., Jin J., Hoshino T., Hanai M., Kobayashi N., Source classification of partial discharge for gas insulated substation using wave shape pattern recognition, *IEEE Trans. Dielect. Electr. Insul.*, 12(2005), No. 2, 374–386
- [2] Zhou Q., Tang J., Tang M., Xie Y., Study on mathematical model for VHF partial discharge of typical insulated defects in GIS, *IEEE Trans. Dielect. Electr. Insul.*, 14(2007), No.1, 30–38
- [3] Iraida K., Igor K., Using electro magnetic PD sensors for diagnostics of high voltage equipment, *Electrical Review*, (2003), No.1
- [4] Barbara F., Pawel Z., Analysis of partial discharge forms in SF6 for diagnostics of GIS, *Electrical Review*, (2005), No.1
- [5] Muresan R.C., Pattern recognition using pulse-coupled neural networks and discrete Fourier transforms, *Neurocomputing*, 51(2003), 487-493
- [6] Godin C., Gordon M. B., Muller J. D., Pattern recognition with spiking neurons-performance enhancement based on a statistical analysis, *IEEE International Joint Conference on Neural Networks*, (1999), 1876-1880
- [7] Karvonen J., A simplified pulse-coupled neural network based sea-ice classifier with graphical interactive training, *Proceedings of the IEEE International Geosciences and Remote Sensing Symposium*, 2(2000), 681-684
- [8] Rughooputh H. C. S., Bootn H., Rughooputh S. D. D. V., Pulse coded neural network for sign recognition for navigation. *IEEE International Conference on Industrial Technology*, 1(2003), 103-105
- [9] Waldemark J., Becanovic V., Lindblad T., Hybrid neural networks for automatic target recognition, *IEEE International Conference on System, Man, and Cybernetics*, 4(1997), 4016-4021
- [10] Johnson J. L., Pulse-coupled neural nets: translation, rotation, scale, distortion, and intensity signal invariance for images, *Applied Optics*, 33(1994), No.26, 6239-6253
- [11] Becanovic V., Kermit M., Eide A. J., Feature extraction from photographic images using a hybrid neural network, *SPIE Proceedings, Ninth Workshop on Virtual Intelligence/ Dynamic Neural network*, 3728(1999), 351-361
- [12] Tang J., Sun C.X., Peng W.X., Extracting partial discharge signals from white noise by wavelet packet transform in GIS, *Automation of Electric Power Systems*, 28(2004), No.5, 25-29
- [13] Xu G.F., Sun C.X., Lu C.H., Compression and Reconstruction for Partial Discharge signals Based on Optimal Wavelet Packets Algorithm Combining with Multi-objective Optimization, *Chinese Journal of Scientific Instrument*, 25(2004), No.1, 57-60
- [14] Iraida K., Juraj K., Roman C., Multi-scale decomposition for partial discharge analysis, *Electrical Review*, (2008), No.9
- [15] Marcin L., Tomasz B., Wavelet analysis of the signals modeling the apparatus used in the acoustic method of partial discharge measurement, *Electrical Review*, (2006), No.1

**Authors:** Jiabin Zhou, State Key Laboratory of Power Transmission Equipment & System Security and New Technology, Chongqing University, Chongqing, 400030. E-mail: zhoujb1986@gmail.com; prof. Ju Tang, State Key Laboratory of Power Transmission Equipment & System Security and New Technology, Chongqing University, Chongqing, 400030. E-mail: cqtangju@vip.sina.com; prof. Xiaoxing Zhang, State Key Laboratory of Power Transmission Equipment & System Security and New Technology, Chongqing University, Chongqing, 400030. E-mail:mikezxx@tom.com; Jiagui Tao, State Key Laboratory of Power Transmission Equipment & System Security and New Technology, Chongqing University, Chongqing, 400030. E-mail: taojiagui@163.com.